IEEE *Access*

Reliable Robot-Flock-Based Monitoring System Design via A Mobile Wireless Sensor Network

PENG ZENG[1], JIAHONG HE[ID][2], AND BINGTUAN GAO[ID][2], (Member, IEEE)
[1]Electric Power Research Institute, Guizhou Power Grid Company Ltd., Guiyang 550007, China
[2]School of Electrical Engineering, Southeast University, Nanjing 210096, China

Corresponding author: Jiahong He (hejiahong@seu.edu.cn)

ABSTRACT The reliable distributed monitoring system provides the real-time video observation from the power cable tunnels when the preinstalled communication system is disabled in an emergency. The spherical robotic prototypes are designed as the sensor node based on the analysis of the robot dynamic model. A novel self-constructed mobile wireless sensor network (MWSN) is proposed to realize the communication and positioning functions through the fusion of the Ad-Hoc and ultra-wideband (UWB) approaches. The Ad-Hoc network consists of multiple robot nodes as sensor carriers and relay stations to transmit large amounts of data from the accident scene to the monitoring terminal. The UWB network consists of UWB tags and bases on each node and implements the leader-follower (LF) strategy to create the robot formation. In order to maximize the monitoring area and maintain the reliability of the network, the traditional LF strategy is optimized based on the *N-X* algorithm subjected to the constraints of node number, Ad-Hoc communication and UWB positioning range, and the power tunnel boundaries. A self-constructed MWSN consisting of five robotic nodes ($N = 5$) is capable of covering 40 m of power cable tunnel, when the value of X is selected as 3. The network failure probability reduces from 73.5% ($X = 0$) to 0.2% ($X = 3$) when the malfunction probability of sensor node is 23.3% due to the accident condition in the tunnel. Finally, the simulation and experimental results show that the optimized LF algorithm increases 20.2% coverage of the network in the curve formation. The network transmits a monitoring video streaming with a 320×240 pixel resolution and a delay less than 150 ms. The real-time video observation from the accident scene is significant to formulate the emergency countermeasure and investigate the direct cause of the accident.

INDEX TERMS Power cable tunnel, monitoring system, spherical robot, mobile wireless sensor network, leader-follower strategy, formation optimization.

I. INTRODUCTION

Underground power cables have gradually replaced traditional overhead lines as the dominant power distribution method in modern cities, because they have ad-vantages in urban planning, transmission reliability, and anti-interference ability [1]. However, power cable breakdown and explosion frequently occur due to the complicated environment of the tunnel. Consequently, fixed and mobile automatic monitoring systems are equipped in the tunnel in order to reduce the risk of inspection opera-tors and improve the inspection efficiency [2]. However, the preinstalled monitoring systems are likely to become disabled due to the

The associate editor coordinating the review of this manuscript and approving it for publication was Qin Liu.

paralyzed communication system, when a fire ignition or cable explosion accident occurs in an enclosed space [3], [4]. Moreover, the severe pass loss and fading of wireless transmission signals in power cable tunnels cause conventional communication and positioning methods like global positioning system (GPS) malfunction [5], [6]. The construction of an independent wireless sensor network (WSN) is a feasible method to solve these problems [7]. Therefore, this paper proposes a monitoring system with multiple sensor nodes to construct a large-bandwidth wireless communication and positioning network. This mobile WSN (MWSN) is capable of transmitting the real-time video from the accident scene in the power cable tunnel.

The spherical robot is the network node as well as a mobile platform to carry the camera terminal. The spherical structure

of the robot node is selected for three reasons according to the specific accident environment of the power cable tunnel. Firstly, the spherical robot is not prone to overturn due to its spherical geometry and low center of gravity in its internal structure, which is suitable for the uneven tunnel surface [8]. In addition, the small rolling friction between the spherical shell and the ground improves its energy efficiency [9], [10]. Moreover, the control and camera modules are integrated inside the shell to protect the modules from the potential threat of accidents in the tunnel and to improve the anti-interference ability of the system [11], [12]. Therefore, the spherical node provides the support for the self-constructed wireless communication network and formation control.

The self-constructed MWSN is the fusion of the Ad-Hoc communication network and the ultra-wideband (UWB) positioning network. Multiple Ad-Hoc and UWB modules carried by the sensor nodes are served as the relay stations and navigating devices for communication and positioning, respectively. On the one hand, the nodes in the Ad-Hoc network can enter and leave the network as long as the minimum number of nodes in the network is satisfied, so that the communication network has characteristics of rapid deployment and strong invulnerability [13]. On the other hand, UWB is a wireless carrier positioning technology to measure the distances between the base and tag with high bandwidth [14], [15], which provides the distance information for each sensor node to optimize the topology of the network.

The positioning network applies the leader-follower (LF) formation strategy to construct the network topology. Since LF strategy only requires the leader information for the follower, it simplifies the network structure and increases the tolerance of the node loss [16]. In order to improve the flock monitoring ability, this article designs a formation optimization strategy to maximize the monitoring coverage area and ensure the reliability of the WSN. The topology of spherical robot flock is optimized every 500 ms, which makes sure that the flock maintains the optimal formation dynamically.

Finally, this paper develops physical prototypes of the proposed system, and experiments are conducted in the power cable tunnel to verify the model accuracy.

The rest of this paper is organized as follows. Section 1 introduces the overall description of the system developed in this paper. Section 2 displays the related works about this article. Section 3 provides the design of the emergency accident monitoring system. Section 4 presents the modelling and prototype design of the sensor node. Section 5 describes the principle of robot flock formation control strategy. Section 6 provides the simulation analysis of the robot flock formation control strategy. Section 7 illustrates the experiment verification of the system. Finally, Section 8 draws the conclusion of the paper.

II. RELATED WORKS

WSNs are used in various applications due to its advantages of flexibility to the environment, cost saving on long distance wires and data security during transmission [17]–[19]. Bhuiyan *et al.* implemented the WSN to monitor the heath and operation status for structures [20]. Rahman *et al.* developed a 3D-Collaborative wireless network with air, water and ground based on communication infrastructures to rescue victims in flood-affected areas [21] . In order to track multiple objectives in the network, many researchers have investigated various algorithms increases the performance of the WSNs. The distributed tracking algorithms were proposed to predict the target's movements in the mobile target tracking [22]. Alqaralleh *et al.* introduced a reliable multi-object tracking model through the methods of deep learning and energy efficient WSN [23]. Liu *et al.* provided the secure search methods and intelligent route plans for the sensor cloud computing [24]. When the WSN is used in a mobile network, the mobility of the node changes the network formation continuously and increases the probability of network failure due to the loss or inappropriate range of nodes [25], [26]. In order to mitigate the impact of node mobility, Zafar proposed two mobility-aware hierarchical clustering algorithms for MWSN based on three-layer clustering hierarchy [27]. Energy efficiency of MWSNs also has a significant impact on the network reliability in a long period [28]–[30]. This paper focuses on the system to realize emergent monitoring function when the accident occurs. LF strategy is implemented according to the boundary geometry of the power cable tunnel.

LF strategy is a widely used method for robot formation control in many fields [16], [31]–[33]. Jia and Wang proposed a distributed flocking algorithm for multiple robotic fishes group to execute the cohesive flocking and formation flocking task on the water surface based on the LF strategy [34]. Xie *et al.* applied LF strategy to the field of new energy power generation, proposed a heliostats cluster control method to improve the control precision and reduce the control cost of solar tower power plants [35]. To prevent the complete disintegration of robot flock, Zheng *et al.* proposed a bidding-based queue control strategy for spherical robot flock to improve the formation's invulnerability when the leader robot is damaged [36]. The accidents in the power cable tunnel creates extremely high temperature or humidity environment, and significantly increases damage probability of sensor nodes. Therefore, this paper optimizes the traditional LF strategy by maximize the coverage range and maintain the reliability of the network.

III. SYSTEM DESCRIPTION

The monitoring system consists of the PC terminal and the mobile spherical robot flock in the power cable tunnel. On the one hand, the PC terminal serves as the information receiving equipment to display the real-time video from the emergent accident scene. On the other hand, the mobile spherical robot flock serves an essential role in data collection, formation movement, and wireless signal transmission. Firstly, each spherical robot carries the camera sensor terminal, which defines its role as the information collecting equipment. Moreover, each robot integrates three UWB modules to

achieve the LF formation control strategy. Eventually, an Ad-Hoc module is integrated in each robot to form the data transmission network (Figure 1).
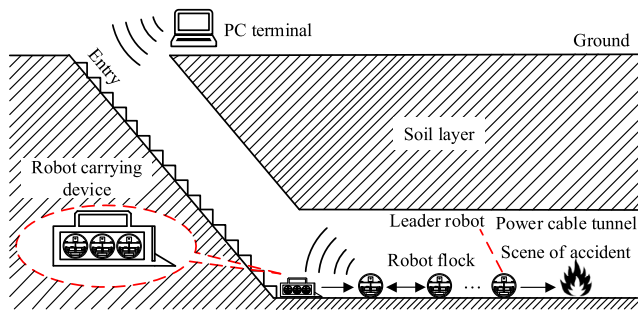

FIGURE 1. Diagram of the monitoring system.

As shown in Figure 1, the operator selects the robot closest to the accident scene as the leader robot under control. Each robot is a relay station for wireless signal transmission. The monitoring information collected by the leader robot is transmitted back to the PC terminal in a multi-hop way. The collected information assists the maintenance personnel to make an emergency plan (Figure 2).

IV. MODELLING AND PROTOTYPE DESIGN OF THE SENSOR NODE

A. DYNAMIC MODELLING OF THE SENSOR NODE

The sensor node adopts a two-wheel differential driving cart as the internal driving system (Figure 3). The rolling of the spherical shell is driven by two forces. Firstly, left driving torques τ_l and right driving torques τ_r are applied to the spherical shell through the friction between the wheels and the spherical shell. In addition, the internal cart generates the vertical inclination θ due to the reaction torque of the spherical shell. Therefore, the gravity of the internal cart also contributes the driving force to the spherical shell. The difference between the two driving torques generates the steering angle φ. The distance between the cart's centroid G and the center of the ball C is l. Φ is the rolling angle of spherical shell.

Euler-Lagrange equation is used to analyze the dynamic model of the spherical robot. The dynamic model consists of seven generalized coordinates that are coupled with each other. Three non-holonomic constraint equations in the model perplex the coupling among those coordinates instead of reducing their amount. Therefore, this paper established the rectilinear motion dynamic model and steering motion dynamic model separately to reduce the model complexity. The number of generalized coordinates is reduced to 3 and non-holonomic constraints are removed in the dynamic model through the separation.

The Euler–Lagrange equation with dissipation function ψ is expressed as

$$\frac{d}{dt}\left(\frac{\partial L}{\partial \dot{q}_j}\right) - \frac{\partial L}{\partial q_j} + \frac{\partial \psi}{\partial q_j} = Q_j \ (j = 1, 2, 3 \cdots, m) \quad (1)$$

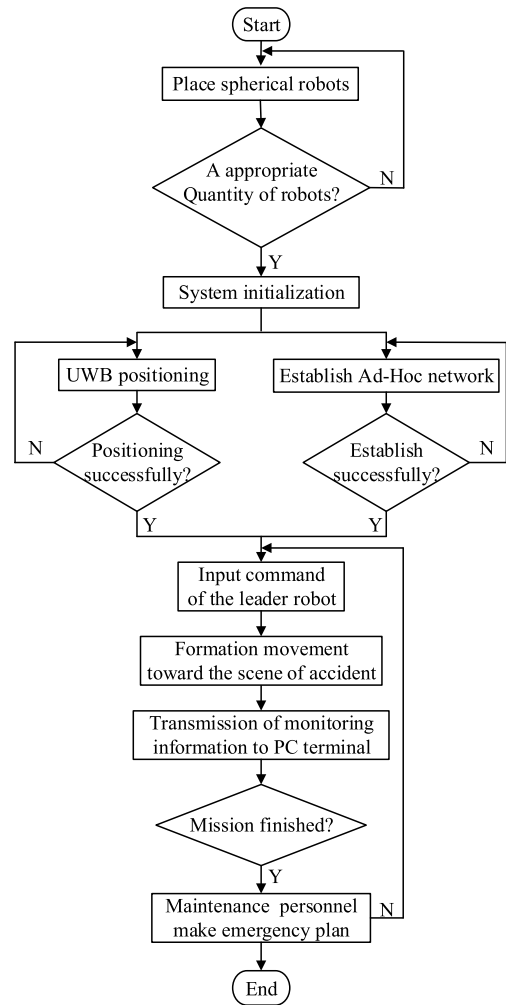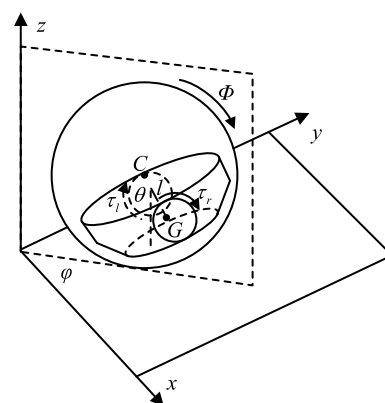**FIGURE 2.** System workflow diagram.

FIGURE 3. Motion diagram of the spherical robot.

where L is the difference between the kinetic energy and potential energy of the system, Q_j is the generalized force corresponding to the number j generalized coordinate.

When the spherical robot performs a zero-radius steering motion, the position of the inner cart's centroid remains

unchanged. The system can be described solely by one parameter φ. Adopt viscous damping coefficient ξ_1 to represent the viscous frictions in motor bearing and between the spherical shell and the wheels during the steering process. The dynamic equation of steering motion is derived as

$$J_m \ddot{\varphi} + \xi_1 \dot{\varphi} = \tau_r - \tau_l \qquad (2)$$

where J_φ is the spherical robot's moment of inertia during the steering motion, $J_\varphi = (md^2 + 2MR^2/3)$.

When the spherical robot performs a rectilinear motion, the position and attitude of the spherical shell can be solely described by Φ due to the complete constraint $x_C = R\Phi$ between the ball center C's abscissa x_C and the rolling angle Φ.

The position and attitude of the internal cart can be solely described by θ due to the complete constraint between the cart's centroid G's position (x_G, z_G) and θ as follows

$$\begin{cases} x_G = x_C + l \sin\theta \\ z_G = R - l \cos\theta \end{cases} \qquad (3)$$

To sum up, the rectilinear motion of spherical robot can be described by two generalized coordinates $q = (\Phi, \theta)^T$.

L is derived as

$$\begin{aligned} L &= T_1 + T_2 - V_1 - V_2 \\ &= (\frac{1}{2}M\dot{x}_C^2 + \frac{1}{2}I\dot{\Phi}^2) + [\frac{1}{2}m\left(\dot{x}_G^2 + \dot{z}_G^2\right) + \frac{1}{2}J_\theta\dot{\theta}^2] \\ &\quad - MgR - mg\left(R - l\cos\theta\right) \end{aligned} \qquad (4)$$

where T_1 and V_1, T_2 and V_2 represent the kinetic energy and potential energy of the spherical shell and the internal cart, respectively. M and m refer to the mass of the spherical shell and the cart, respectively. R refers to the radius of the shell. I is mass of the spherical shell moment of inertia, $I = 2MR^2/3$. J_θ is the moment of inertia of the cart's centroid around the sphere center, $J_\theta = ml^2$.

$$\begin{cases} Q_\Phi = \tau_r + \tau_l + F_f \cdot R \\ Q_\theta = \tau_r + \tau_l \end{cases} \qquad (5)$$

where F_f is the rolling friction between the ground and the spherical shell, $F_f = \mu\left(M + m\right)g \cdot sgn(\dot{\Phi})$. $sgn(\dot{\Phi})$ is the direction function limiting the direction of friction always opposite to the rolling direction of the spherical robot. μ is the rolling friction coefficient.

Adopt viscous damping coefficient ξ_2 to represent the viscous frictions during the rectilinear motion process. The dissipation function is derived as

$$\psi = \frac{1}{2}\xi_2(\dot{\theta} + \dot{\Phi})^2 \qquad (6)$$

Combining the equation 1 and 3-6, the dynamic equation of rectilinear motion is expressed as

$$\begin{cases} \left(\frac{5}{3}M + m\right)R^2\ddot{\Phi} + mRl\cos\theta \cdot \ddot{\theta} - mRl\sin\theta \cdot \dot{\theta}^2 \\ +\xi_2(\dot{\Phi} + \dot{\theta}) = \tau_r + \tau_l - \mu\left(M + m\right)g \cdot sgn(\dot{\Phi}) \cdot R \\ 2ml^2\ddot{\theta} + mRl\cos\theta \cdot \ddot{\Phi} + mgl\sin\theta \\ +\xi_2(\dot{\theta} + \dot{\Phi}) = \tau_r + \tau_l \end{cases} \qquad (7)$$

B. HARDWARE DESIGN OF THE PHYSICAL PROTOTYPE

According to the dynamic model, the parameters of the robot prototypes are determined and shown in Table 1. It can be observed that the prototype has the advantages of portability and low cost, which is suitable to serve as a consumable device to deal with emergencies.

TABLE 1. Parameters of the physical prototype.

Parameter of the spherical robot	Value
diameter / m	0.16
weight / kg	0.3
working hours / h	5
cost / yuan	1500
maximum speed / m/s	0.8
optimal distance / m	$0.2 < d^* < 30$

In Table 1, optimal distance refers to following distance between two adjacent robots in the formation. It is illustrated in section 5.

Figure 4 presents the mechanical structure of the wheel-driven spherical robot composed of two parts: the external transparent spherical shell and the internal cart. The shell provides support and protection for the internal cart from possible damage in the power cable tunnel. The structure of the internal cart consists of multiple layers, including the UWB platform, motor layer, and battery layer located from top to bottom. Two-wheel driving structure realizes the zero-radius steering in a narrow space. The combined structure has an anti-toppling ability to ensure the movement of the robot in complicated tunnel conditions.
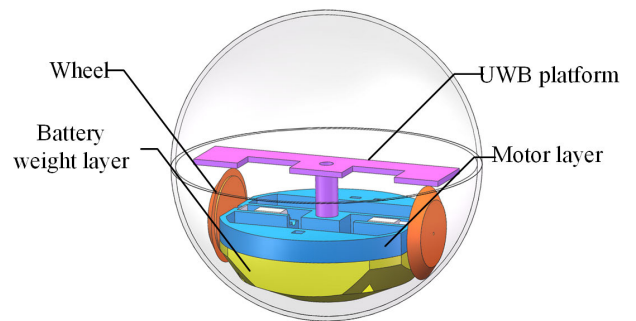

FIGURE 4. Mechanical structure of the wheel-drive spherical robot.

The structure of the internal cart is introduced from top to bottom as follows. The UWB platform supports the tracking and ranging between spherical robot nodes. Three UWB modules is located at the middle and both ends of the platform. The independent DC motors drive the wheels under the control of the microprocessor unit. The Ad-Hoc communication module and the camera sensor terminal are responsible for real-time video collection and transmission. The power consumption of each module for the robot node is listed in Table 2.

TABLE 2. The power consumption of each module in the robot.

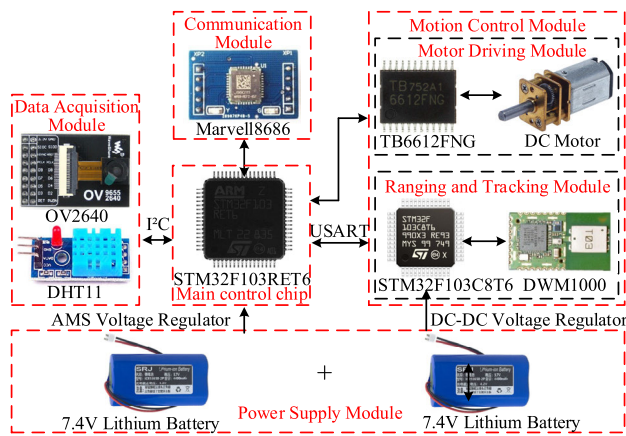| Module	Model	Power (mW)
Processor 1	STM32F103RET6	500
Processor 2×3	STM32F103C8T6	1200
Ad-Hoc	Marvell8686	875
UWB×3	DWM1000	1245
Camera	OV2640	140
Motor driver	TB6612FNG	890
Voltage regulator 1	LM2596T-3.3	37
Voltage regulator 2	AMS1117	56
Motor×2	GA12-N20	720
Total		**5663**

FIGURE 5. The structure diagram of the mobile node measurement and control circuit system.

Therefore, the battery weight layer is equipped with two 7.4 V/3000 mAh lithium batteries to ensure continuous movement and monitoring for 6.9 hours. To maintain voltage stability and avoid the chip's overheating, each robot node's continuous working time is limited less than 5 hours. In addition, a counterweight slot at the bottom of the battery slot is designed to lower the center of gravity of the spherical robot.

Figure 5 shows the structure diagram of the spherical robot's measurement and control circuit system.

V. ROBOT FLOCK FORMATION CONTROL STRATEGY

Spherical robot formation control utilizes a formation optimization strategy based on LF formation method to explore the power cable tunnel during an emergent accident. The aim of this strategy is to maximize the monitoring area and maintain the communication network reliability when one of the nodes drops out from the flock.

A. ROBOT FLOCK KINEMATIC MODEL BASED ON LF STRATEGY

LF strategy is a decentralized formation control method (Figure 6). Every two adjacent robots form a LF structure, and the follower robot adjusts its motion to track the leader robot according to leader robot's position information, which is extended to the whole flock by analogy [31]. The follower
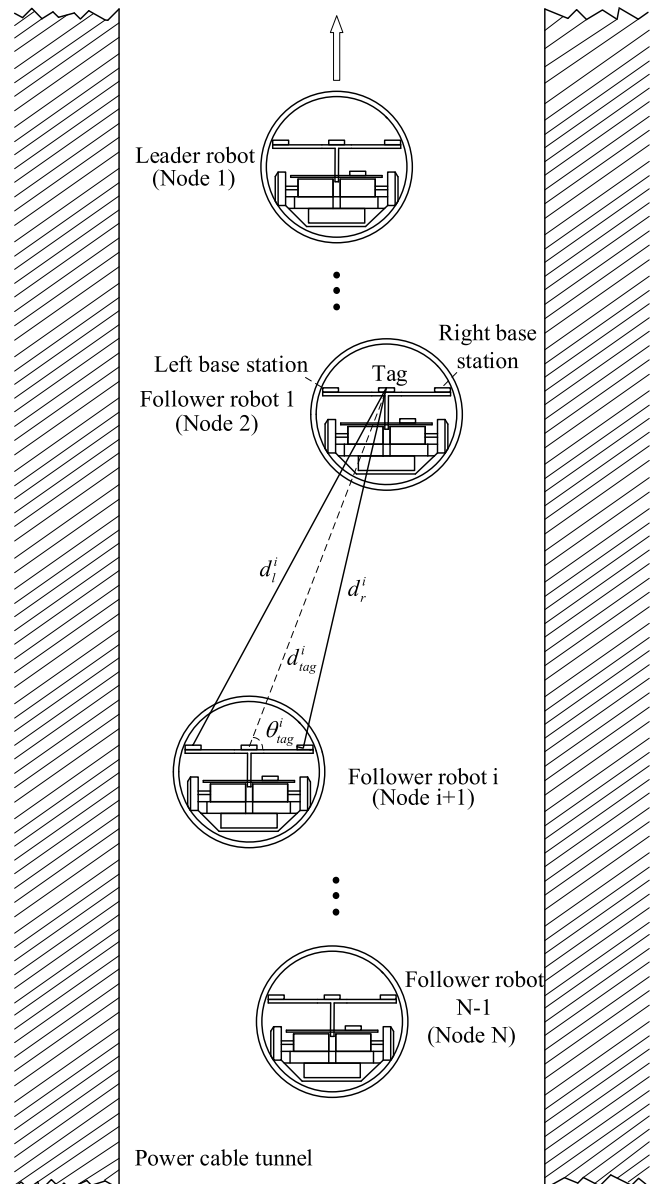

FIGURE 6. Diagram of the line formation following strategy based on the UWB ranging method.

robots are served as the data transmission relay nodes and the potential leader in case that the leader is damaged in the accident.

The follower robot uses UWB positioning technology to locate the leader robot. Each robot is equipped with three UWB modules, the middle module serves as the tag, and the modules on both sides serve as the base stations. The distance d_i tag and the angle θ_i tag between two tags represent the distance L_{lf} and angle θ_f between two robots. The distance between the left (or right) base stations of the follower robot and the tag of the leader robot is d_l^i (or d_r^i), and the distance between the two base stations is measured as L_{rl}. The distance L_{lf} and angle θ_f are calculated according to the robot geometry.

The schematic diagram of the LF method is shown in Figure 7. The kinematic equation of the leader robot is obtained from the geometric relationship:

$$\dot{p}_l = \begin{bmatrix} \dot{x}_l \\ \dot{y}_l \\ \dot{\theta}_l \end{bmatrix} = \begin{bmatrix} \cos\theta_l & 0 \\ \sin\theta_l & 0 \\ 0 & 1 \end{bmatrix} \begin{bmatrix} v_l \\ \omega_l \end{bmatrix} \qquad (8)$$
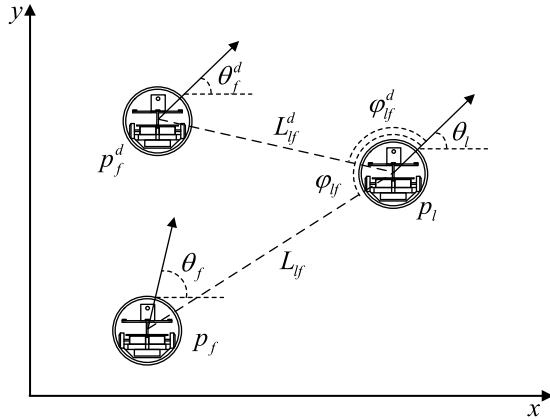

FIGURE 7. The schematic diagram of robot's kinematic model based on LF strategy.

The target position p_f^d and current position p_f of the follower robot are formulated as

$$p_f^d = \begin{bmatrix} x_f^d \\ y_f^d \\ \theta_f^d \end{bmatrix} = \begin{bmatrix} x_l + L_{lf}^d \cos(\varphi_{lf}^d + \theta_l) \\ y_l + L_{lf}^d \sin(\varphi_{lf}^d + \theta_l) \\ \theta_l \end{bmatrix} \qquad (9)$$

$$p_f = \begin{bmatrix} x_f \\ y_f \\ \theta_f \end{bmatrix} = \begin{bmatrix} x_l + L_{lf} \cos(\varphi_{lf} + \theta_l) \\ y_l + L_{lf} \sin(\varphi_{lf} + \theta_l) \\ \theta_f \end{bmatrix} \qquad (10)$$

The inertial coordinate system OXY is selected as the reference frame, and the body coordinate system $O_f X_f Y_f$ is attached to the follower robot itself, in which the direction X_f is the velocity direction and Y_f is the vertical direction of the velocity. x_e, y_e are used to represent the distance error between the follower robot and the leader robot in the X_f direction and Y_f direction respectively, and θ_e is the angle error.

$$e_{lf} = \begin{bmatrix} x_e \\ y_e \\ \theta_e \end{bmatrix} = \begin{bmatrix} \cos\theta_f & \sin\theta_f & 0 \\ -\sin\theta_f & \cos\theta_f & 0 \\ 0 & 0 & 1 \end{bmatrix} \begin{bmatrix} x_f^d - x_f \\ y_f^d - y_f \\ \theta_f^d - \theta_f \end{bmatrix} \qquad (11)$$

Substitute equation 9 and equation 10, equation 11 can be rewritten as

$$e_{lf} = \begin{bmatrix} x_e \\ y_e \\ \theta_e \end{bmatrix} = \begin{bmatrix} L_{lf}^d \cos(\varphi_{lf}^d + \theta_{lf}) - L_{lf} \cos(\varphi_{lf} + \theta_{lf}) \\ L_{lf}^d \sin(\varphi_{lf}^d + \theta_{lf}) - L_{lf} \sin(\varphi_{lf} + \theta_{lf}) \\ \theta_f^d - \theta_f \end{bmatrix}$$
$$(12)$$

where $\theta_{lf} = \theta_l - \theta_f$.

The optimization goal is to reduce errors close to 0, which is formulated as

$$\lim_{t \to \infty} e_{l_i f_{i+1}}(t) = 0 \quad (i = 1, 2, \cdots, N) \qquad (13)$$

B. LF STRATEGY OPTIMIZATION BASED ON N−X ALGORITHM

The mobile wireless Ad-Hoc network can automatically form a new topology with other undamaged nodes to ensure the adjacent robot within the communication range, when one of the nodes drops out of the network, the network (Figure 8).
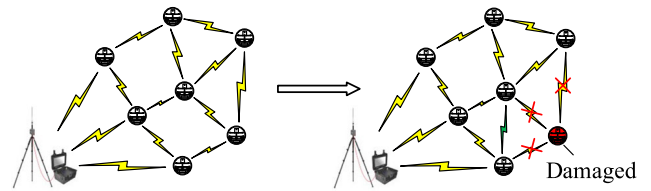

FIGURE 8. Schematic diagram of Ad-Hoc network's invulnerability.

In order to maximize the coverage and improve the reliability of the mobile network, a formation optimization is designed based on LF strategy to create an approximately one-dimensional linear structure of robot flock according to the long and narrow geometry of the power cable tunnel. The LF strategy is optimized according to the $N - X$ algorithm to insure the reliable communication when X robot nodes drop off from the flock. The optimization objective is formulated as

$$max \int_0^{T_t} \int_0^L F(x, t) dx dt \qquad (14)$$

where T_t is the total operation time, L is the range constraint and $F(x, t)$ refers to the continuous trajectories of the robot flock. According to the periodic control and number of robot nodes, Equation 10 is discretized as

$$max \sum_{k=1}^{K} \sum_{n=1}^{N} \| f(n+1, (k+1)T_p) - f(n, kT_p) \| \qquad (15)$$

where K is the number of control period since the initial state, N is the number of robot nodes, T_p is the control period and $f(n, kT_p)$ refers to the coordinates of robot node n at k^{th} control period subjected to the following constraints.

The movement of the spherical robot in power cable tunnel is subject to four constraints. The first constraint is the geometric constraint of the power cable tunnel's motion plane. The movement of the spherical robot is limited within the power cable tunnel. The radius of the power cable tunnel is R, the diameter of the drainage ditch on both sides is d, set security margin is M, then the constraint is formulated as

$$-R + d + M \le x_i \le R - d - M \quad (i = 1, 2, \cdots, N) \qquad (16)$$

On one hand, the distance between two adjacent monitoring robots cannot exceed the positioning range of UWB module. On the other and, the robot flock topology needs to satisfy

the network stability constraints to ensure the reliability of the network. The $N - X$ algorithm is proposed and applied for the constraints of Ad-Hoc and UWB communication ranges. The algorithm is described as follows. The communication range of each spherical robot covers $X + 1$ number of adjacent robot nodes. Therefore, the remaining functional robots can communicate directly to ensure the integrity of the network, when the intermediate robots are disabled in the network.

The positioning range of UWB chip is Dst_{UWB}, the positioning constraint is formulated as

$$0 \leq |y_{i+x+1} - y_i| \leq Dst_{UWB} \quad (i = 1, 2, \cdots, N-1) \quad (17)$$

The maximum positioning range of UWB module is 55 m according to the measurement results in the environment of underground power cable tunnel. Therefore, Dst_{UWB} is set as 50 m to ensure the reliability of UWB communication.

The communication range of Ad-Hoc module is Dst_{WiFi}, the network stability constraint is formulated as

$$0 \leq |y_{i+x+1} - y_i| \leq Dst_{WiFi} \quad (i = 1, 2, \cdots, N-2) \quad (18)$$

The maximum communication range of Ad-Hoc chip is 35 m according to the measurement results. Therefore, Dst_{WiFi} is set as 30 m to ensure the stability of Ad-Hoc communication.

According to the $N - X$ strategy, the maximum optimal distance between two adjacent robots is set as Dst_{WiFi}/X. Therefore, the maximum coverage of N robot nodes $S_{CoverMax}$ is

$$S_{CoverMax} = (N-1)\frac{Dst_{WiFi}}{X} \quad (19)$$

The mobile wireless network failure probability is calculated as

$$P_{Network} = \sum_{n=X+1}^{N} (N-n)(P_{Node})^n (1 - P_{Node})^{N-n} \quad (20)$$

where P_{Node} is the malfunction probability of sensor node. Through the test under the accident condition in the power cable tunnel, the value of P_{Node} is set as 23.3%.

The values of $S_{CoverMax}$ and P_{Node} are shown in Table 3 when the total number of sensor nodes is 5. It can be seen that there is a negative correlation between $S_{CoverMax}$ and P_{Node}.

TABLE 3. The values of $S_{CoverMax}$ and P_{Node} under different X value.

X	$S_{CoverMax}$ (m)	P_{Node}
0	240	73.5%
1	120	9.1%
2	60	1.7%
3	40	0.2%

Table 3 indicates that the network failure probability reduces from 73.5% to 0.2% as the value of X increases from 0 to 3. Therefore, the value of X is selected as 3 to enhance the network reliability in the emergent condition of the power cable tunnel.

VI. SIMULATION RESULTS

Straight lines and curves are the typical structures of the power cable tunnel. The robot formations in above two structures are simulated to evaluate the performance of the formation optimization strategy. Five sensor nodes are placed in the power tunnel in order as the initial state. In the simulation, the optimal distance between adjacent sensor nodes is set as 1.5 m to observe the trajectories and evaluate the optimization performance of the MWSN in line and curve formation movements.

A. LINE FORMATION OPTIMIZATION

The optimal result of line formation optimization is shown in Figure 9. The simulation model is designed based on the boundary geometry of the actual power cable tunnel. The solid lines on both sides represent the wall of the power cable tunnel, the area between the dotted line and the solid line is the drainage ditch on both sides of the power cable tunnel, and the area between the two dotted lines is the area for the robot operation.
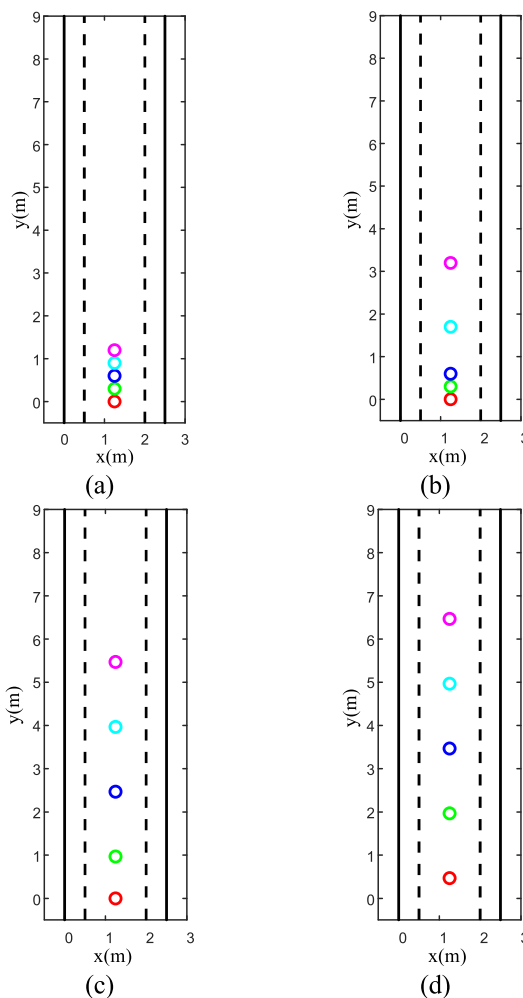

FIGURE 9. The result of line formation optimization. (a) Initial state; (b) Flock state at 5 s; (c) Flock state at 10 s; (d) Flock state at 13 s.

Figure 9 (a) is the initial state with static robot flock in a line formation. Figure 9 (b) shows that the leader robot first moves in a straight line in the power cable tunnel controlled by the PC terminal. After the distance between the leader robot and its follower robot reaches the optimal distance, the follower robot begins to follow the leader robot. Then, the second follower robot starts to move after the distance between the first follower robot and the second follower robot reaches the optimal distance, which expands to the whole formation by analogy (Figure 9 (c)), and finally forms the optimal formation shown in Figure 9 (d).

B. CURVE FORMATION OPTIMIZATION

The optimal result of curve formation optimization is shown in Figure 10, where (a) is the same initial state with the line formation optimization. The leader robot is set at the entrance of the curve. Figure 10 (b) shows that after starting the formation optimization, the leader robot starts to move in the power cable tunnel under the control of the PC terminal. In order to enable the spherical robot formation to pass the curve with the shortest path, we control the leader robot to move along the border of the curve. The follower robot follows its leader robot in turn, and its movement in the curve is also close to the border of the curve (Figure 10 (c)). Finally, Figure 10 (d) shows that the spherical robot formation forms an optimal formation through the curve. The simulation results show that the coverage of the network increases 21.7% when compared to the results without the optimized LF strategy in curve formation.
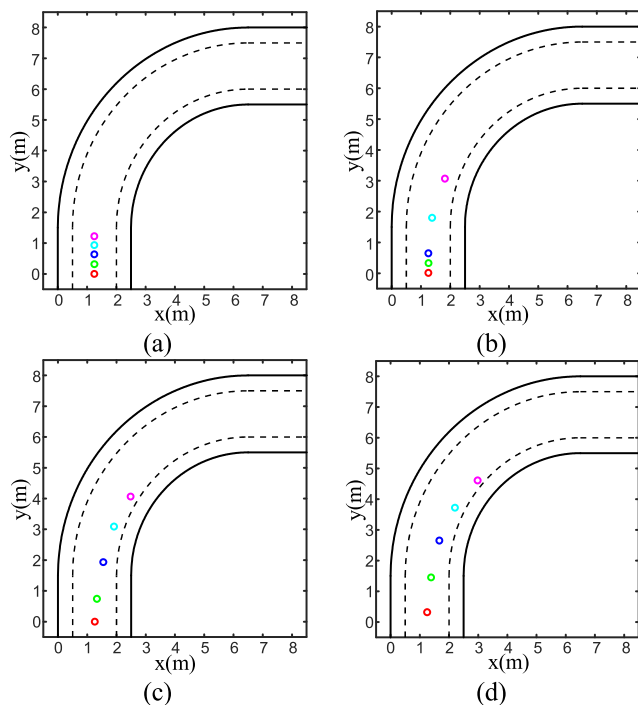
FIGURE 10. The result of curve formation optimization. (a) Initial state; (b) Flock state at 5 s; (c) Flock state at 10 s; (d) Flock state at 13 s.

VII. EXPERIMENTAL RESULTS

Both straight line and curve formation optimization experiments are conducted in the power cable tunnel. The power cable tunnel is 2.5 m wide, and the drainage ditches on both sides are 0.5 m wide. Above the drainage ditches, eight power cables with different voltage levels are placed on the support frame. The initial conditions are exactly the same as the simulation.

A. LINE FORMATION OPTIMIZATION

The experimental results of the line formation optimization are shown in Figure 11. The experimental initial state parameters are consistent with the simulation. The position of the spherical robot formation is captured by a camera every 1 s. The leader robot first makes a rectilinear motion in the power cable tunnel under the control of the PC terminal, and then the other robots follow each other in turn when the distance between them reaches the optimal distance. Finally, the spherical robot group performs the monitoring task in the power cable tunnel in the form of line optimal formation.
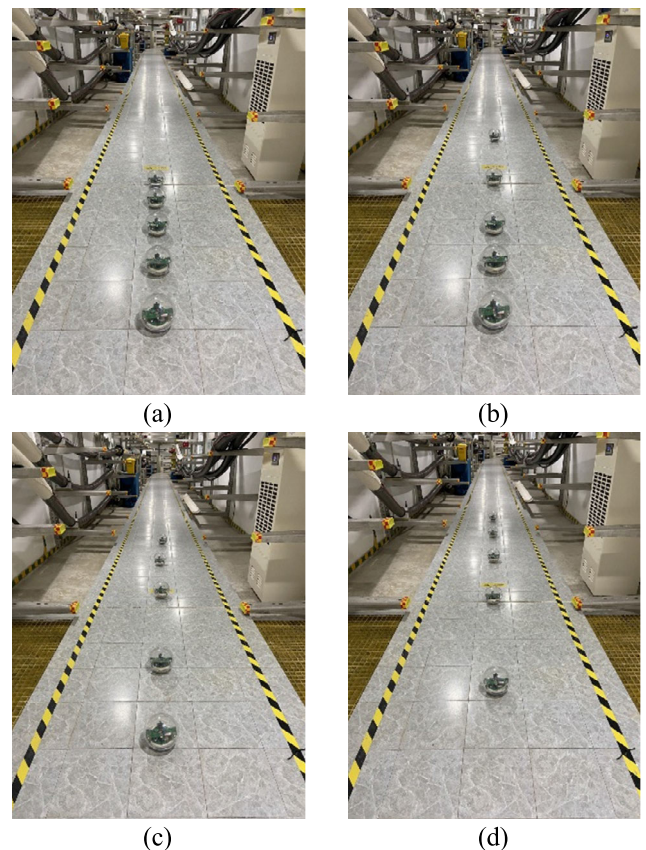
FIGURE 11. The experimental result of line formation optimization. (a) Initial state; (b) Flock state at 5 s; (c) Flock state at 10 s; (d) Flock state at 13 s.

The experimental trajectories of the robots are divided into *x*-axis and *y*-axis displacements (Figure 12). The simulation results are compared with the experimental results. Table 4 shows the *x*-axis and *y*-axis displacement errors in the line formation optimization experiment.
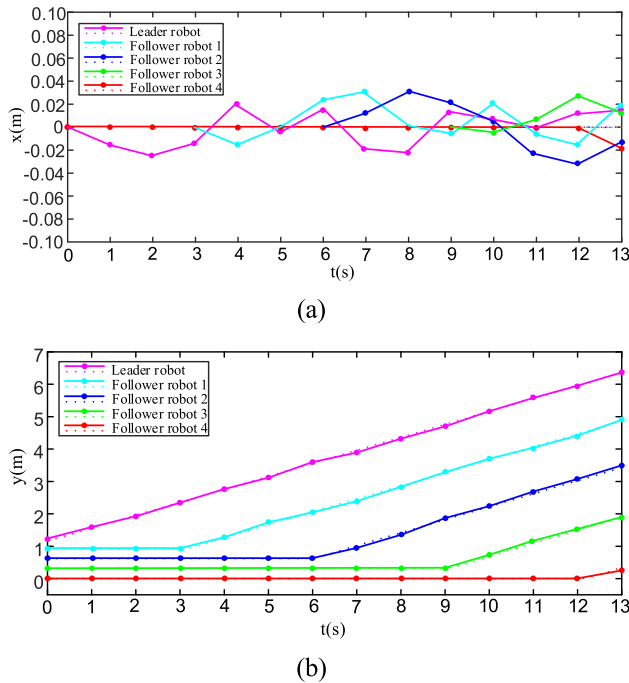
(a)

(b)

FIGURE 12. Results of the line formation optimization experiment. (a) The displacement of robots on the x-axis; (b) The displacement of robots on the y-axis.

TABLE 4. Errors in line formation following experiment.

Spherical robot	Average error $|\Delta x|/|\Delta y|$(m)	Maximum error $|\Delta x|/|\Delta y|$(m)
Leader robot	0.01/0.03	0.02/0.04
Follower robot 1	0.02/0.04	0.03/0.05
Follower robot 2	0.02/0.05	0.03/0.06
Follower robot 3	0.01/0.04	0.02/0.06
Follower robot 4	0.02/0.04	0.02/0.04

Figure 12 shows that the simulation and experimental results remain consistent. However, the disturbances exist during the experiment for the following reasons. First, the positioning error using the proposed UWB positioning method amplifies with the increase of the distance between robots. The uneven ground and the obstacles in the power cable tunnel also affect the control reliability. As shown in Table 4, the line formation errors on the x-axis $|\Delta x|$ and y-axis $|\Delta y|$ were less than 0.03 m and 0.06 m, respectively. Compared with the half of the power cable tunnel's width (1.25 m) and the optimal distance between adjacent robot nodes (1.5 m), the relative errors of $|\delta x|$ and $|\delta y|$ are 2.4% and 4%. The disturbances have little effects on the robot formation control, because the errors are relatively small when compared with the geometric dimension of the power cable tunnel.

B. CURVE FORMATION OPTIMIZATION

The experimental result of the curve formation optimization is shown in Figure 13. Figure 13 indicates that the leader robot
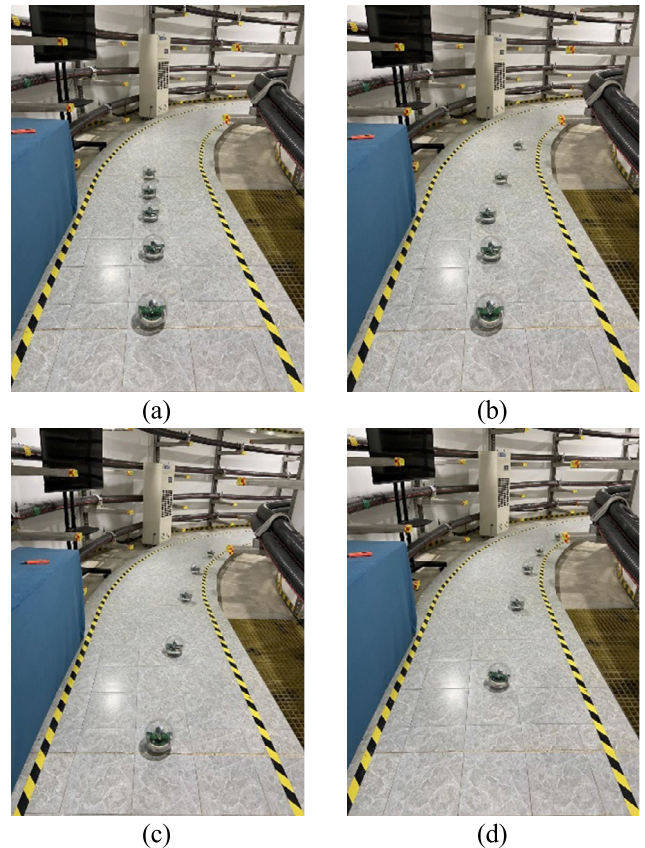

(a)

(b)

(c)

(d)

FIGURE 13. The experimental result of curve formation optimization. (a) Initial state; (b) Flock state at 5 s; (c) Flock state at 10 s; (d) Flock state at 13 s.

first moves to one side and moves along the border of the drainage ditch in the power cable tunnel under the control of the PC terminal. The follower robots follow each other in turn. Eventually, the spherical robot group performs the monitoring task in the power cable tunnel in the form of curve optimal formation.

Similar to Figure 12, Figure 14 presents a comparison between the results of the simulation and experiment for curve formation optimization. The experimental results show that the coverage of the network increases 20.2% when compared to the results without the optimized LF strategy in curve formation, which verifies the simulation result.

As shown in Table 5, the curve formation errors on the x-axis $|\Delta x|$ and y-axis $|\Delta y|$ were less than 0.05 m and 0.07 m, respectively. Similarly, the relative errors of $|\delta x|$ and $|\delta y|$ are 4% and 4.7% respectively. It is concluded that the control reliability of the proposed system was competent for the detection mission in the power cable tunnels because the dimension of the power cable tunnel could tolerate the errors.

During the process of the formation optimization experiment, the PC terminal showed a monitoring video streaming captured by the monitoring robot in a 320 × 240 pixel resolution instantaneously. The average delay of video transmission was less than 150 ms.

TABLE 5. Errors in curve formation following experiment.

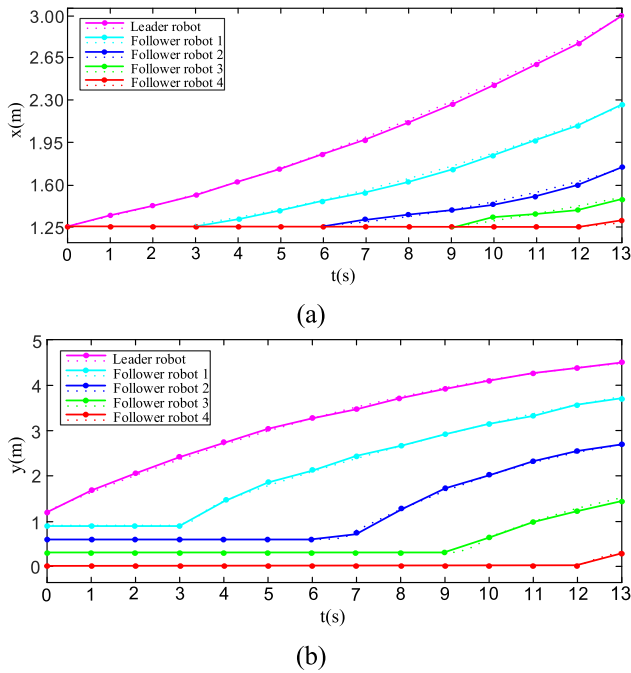| Spherical robot	Average error $\|\Delta x\|/\|\Delta y\|$(m)	Maximum error $\|\Delta x\|/\|\Delta y\|$(m)
Leader robot	0.01/0.04	0.03/0.05
Follower robot 1	0.02/0.05	0.04/0.06
Follower robot 2	0.03/0.04	0.05/0.06
Follower robot 3	0.02/0.06	0.04/0.07
Follower robot 4	0.03/0.03	0.03/0.03

FIGURE 14. Results of the curve formation optimization experiment. (a) The displacement of robots on the x-axis; (b) The displacement of robots on the y-axis.

VIII. CONCLUSION

This paper illustrates the theory and application of a novel self-constructed MWSN based on the fusion of Ad-Hoc and mobile network. The dynamic model for the sensor robotic node demonstrates the advantages of spherical geometry on flexible movement and anti-toppling ability in a narrow environment. The Ad-Hoc relays and UWB stations are integrated to create a MWSN with the communication and positioning functions. The communication network consisting of five robots is capable of covering 40 m of power cable tunnel. The implementation of $N - X$ algorithm significantly increases the reliability of the network and reduces network failure probability from 73.5% ($X = 0$) to 0.2% ($X = 3$). The network transmits a monitoring video streaming with a 320×240 pixel resolution and a delay less than 150 ms. The robot flock topology of the network is determined by the formation optimization method based on LF strategy, which increases 20.2% coverage of the network in curve formation of the power cable tunnel. The real-time video observation from the accident scene is significant to formulate the emergency countermeasure and investigate the direct cause of the

accident. Therefore, the proposed system compensates for the insufficiency of traditional monitoring methods in power cable tunnels when the preinstalled network is disabled.

REFERENCES

[1] Y. Chen, D. Zhang, J. Chen, K. Liu, and F. Yang, "A new fire protection system of power cable tunnel based on wireless sensor network monitoring system," in *Proc. IEEE 11th Conf. Ind. Electron. Appl. (ICIEA)*, Hefei, China, Jun. 2016, pp. 1103–1106.

[2] H. M. Pereira, E. F. Steennis, M. Borges Pinheiro, M. Marques, T. Raczy, R. Palhares, and P. M. F. Almeida, "Partial discharge on-line monitoring in MV underground power cables as part of condition based maintenance strategy," in *Proc. 22nd Int. Conf. Exhib. Electr. Distrib. (CIRED)*, Stockholm, Sweden, 2013, pp. 1–4.

[3] P. Lin, Q. Li, Q. Fan, X. Gao, and S. Hu, "A real-time location-based services system using WiFi fingerprinting algorithm for safety risk assessment of workers in tunnels," *Math. Problems Eng.*, vol. 2014, pp. 1–10, Apr. 2014.

[4] K. Loupos, A. D. Doulamis, C. Stentoumis, E. Protopapadakis, K. Makantasis, N. D. Doulamis, A. Amditis, P. Chrobocinski, J. Victores, R. Montero, E. Menendez, C. Balaguer, R. Lopez, M. Cantero, R. Navarro, A. Roncaglia, L. Belsito, S. Camarinopoulos, N. Komodakis, and P. Singh, "Autonomous robotic system for tunnel structural inspection and assessment," *Int. J. Intell. Robot. Appl.*, vol. 2, no. 1, pp. 43–66, Mar. 2018.

[5] C. B. Wong, E. F. Yang, X. T. Yan, and D. B. Gu, "Autonomous robots for harsh environments: A holistic overview of current solutions and ongoing challenges," *Syst. Sci. Control Eng.*, vol. 6, no. 1, pp. 213–219, Jan. 2018.

[6] C. Jing, B. Zhou, N. Kim, and Y. Kim, "Performance evaluation of an indoor positioning scheme using infrared motion sensors," *Information*, vol. 5, no. 4, pp. 548–557, Oct. 2014.

[7] D. Zhang, Z. Fang, H. Sun, and J. Cao, "HTCRL: A range-free location algorithm based on homothetic triangle cyclic refinement in wireless sensor networks," *Information*, vol. 8, no. 2, pp. 40–44, 2017.

[8] S. Asiri, F. Khademianzadeh, A. Monadjemi, and P. Moallem, "The design and development of a dynamic model of a low-power consumption, two-pendulum spherical robot," *IEEE/ASME Trans. Mechatronics*, vol. 24, no. 5, pp. 2406–2415, Oct. 2019.

[9] T. Urakubo, M. Monno, S. Maekawa, and H. Tamaki, "Dynamic modeling and controller design for a spherical rolling robot equipped with a gyro," *IEEE Trans. Control Syst. Technol.*, vol. 24, no. 5, pp. 1669–1679, Sep. 2016.

[10] B. P. DeJong, E. Karadogan, K. Yelamarthi, and J. Hasbany, "Design and analysis of a four-pendulum omnidirectional spherical robot," *J. Intell. Robotic Syst.*, vol. 86, no. 1, pp. 3–15, Apr. 2017.

[11] C. Camicia, F. Conticelli, and A. Bicchi, "Nonholonomic kinematics and dynamics of the sphericle," in *Proc. IEEE/RSJ Int. Conf. Intell. Robots Syst. (IROS)*, Takamatsu, Japan, vol. 1, May 2000, pp. 805–810.

[12] S. Sabet, M. Poursina, P. E. Nikravesh, P. Reverdy, and A.-A. Agha-Mohammadi, "Dynamic modeling, energy analysis, and path planning of spherical robots on uneven terrains," *IEEE Robot. Autom. Lett.*, vol. 5, no. 4, pp. 6049–6056, Oct. 2020.

[13] N. Heo and P. K. Varshney, "Energy-efficient deployment of intelligent mobile sensor networks," *IEEE Trans. Syst., Man, Cybern. A, Syst. Humans*, vol. 35, no. 1, pp. 78–92, Jan. 2005.

[14] M. Sakr, A. Masiero, and N. El-Sheimy, "LocSpeck: A collaborative and distributed positioning system for asymmetric nodes based on UWB ad-hoc network and Wi-Fi fingerprinting," *Sensors*, vol. 20, no. 1, p. 78, Dec. 2019.

[15] S. Monica and G. Ferrari, "UWB-based localization in large indoor scenarios: Optimized placement of anchor nodes," *IEEE Trans. Aerosp. Electron. Syst.*, vol. 51, no. 2, pp. 987–999, Apr. 2015.

[16] C. L. P. Chen, D. Yu, and L. Liu, "Automatic leader-follower persistent formation control for autonomous surface vehicles," *IEEE Access*, vol. 7, pp. 12146–12155, 2019.

[17] T. Peng, Q. Liu, and G. Wang, "A multilevel access control scheme for data security in transparent computing," *Comput. Sci. Eng.*, vol. 19, no. 1, pp. 46–53, Jan. 2017.

[18] Q. Liu, G. Wang, J. Wu, and W. Chang, "User-controlled security mechanism in data-centric clouds," in *Proc. IEEE 17th Int. Conf. High Perform. Comput. Commun. 7th Int. Symp. Cyberspace Saf. Secur., IEEE 12th Int. Conf. Embedded Softw. Syst.*, New York, NY, USA, Aug. 2015, pp. 647–653.

[19] X. Xu, Q. Huang, H. Zhu, S. Sharma, X. Zhang, L. Qi, and M. Z. A. Bhuiyan, "Secure service offloading for Internet of vehicles in SDN-enabled mobile edge computing," *IEEE Trans. Intell. Transp. Syst.*, early access, Dec. 9, 2020, doi: 10.1109/TITS.2020.3034197.

[20] C. Wang, J. Wu, X. Zheng, B. Pei, X. Zhang, D. Yu, and J. Tang, "Leveraging ICN with network sensing for intelligent transportation systems: A dynamic naming approach," *IEEE Sensors J.*, early access, Jun. 25, 2020, doi: 10.1109/JSEN.2020.3004839.

[21] M. Z. A. Bhuiyan, G. Wang, J. Cao, and J. Wu, "Deploying wireless sensor networks with fault-tolerance for structural health monitoring," *IEEE Trans. Comput.*, vol. 64, no. 2, pp. 382–395, Feb. 2015.

[22] M. Z. A. Bhuiyan, G. Wang, and A. V. Vasilakos, "Local area prediction-based mobile target tracking in wireless sensor networks," *IEEE Trans. Comput.*, vol. 64, no. 7, pp. 1968–1982, Jul. 2015.

[23] M. A. Rahman, M. M. Hasan, A. T. Asyhari, and M. Z. A. Bhuiyan, "A 3D-collaborative wireless network: Towards resilient communication for rescuing flood victims," in *Proc. IEEE 15th Intl Conf Dependable, Autonomic Secure Comput., 15th Int. Conf. Pervasive Intell. Comput., 3rd Int. Conf. Big Data Intell. Comput. Cyber Sci. Technol. Congr. (DASC/PiCom/DataCom/CyberSciTech)*, Orlando, FL, USA, Nov. 2017, pp. 385–390.

[24] Q. Liu, P. Hou, G. Wang, T. Peng, and S. Zhang, "Intelligent route planning on large road networks with efficiency and privacy," *J. Parallel Distrib. Comput.*, vol. 133, pp. 93–106, Nov. 2019.

[25] V. Nazarzehi, A. V. Savkin, and A. Baranzadeh, "Distributed 3D dynamic search coverage for mobile wireless sensor networks," *IEEE Commun. Lett.*, vol. 19, no. 4, pp. 633–636, Apr. 2015.

[26] T. Cheng and A. Savkin, "A distributed self-deployment algorithm for the coverage of mobile wireless sensor networks," *IEEE Commun. Lett.*, vol. 13, no. 11, pp. 877–879, Nov. 2009.

[27] S. Zafar, A. Bashir, and S. A. Chaudhry, "Mobility-aware hierarchical clustering in mobile wireless sensor networks," *IEEE Access*, vol. 7, pp. 20394–20403, 2019.

[28] M. Zhao, J. Li, and Y. Yang, "A framework of joint mobile energy replenishment and data gathering in wireless rechargeable sensor networks," *IEEE Trans. Mobile Comput.*, vol. 13, no. 12, pp. 2689–2705, Dec. 2014.

[29] J.-W. Lin, P. R. Chelliah, M.-C. Hsu, and J.-X. Hou, "Efficient fault-tolerant routing in IoT wireless sensor networks based on bipartite-flow graph modeling," *IEEE Access*, vol. 7, pp. 14022–14034, 2019.

[30] M. K. Naeem, M. Patwary, and M. Abdel-Maguid, "Universal and dynamic clustering scheme for energy constrained cooperative wireless sensor networks," *IEEE Access*, vol. 5, pp. 12318–12337, 2017.

[31] S.-L. Dai, S. He, X. Chen, and X. Jin, "Adaptive leader–follower formation control of nonholonomic mobile robots with prescribed transient and steady-state performance," *IEEE Trans. Ind. Informat.*, vol. 16, no. 6, pp. 3662–3671, Jun. 2020.

[32] X. Li, S. Xu, H. Gao, and H. Cai, "Distributed tracking of leader-follower multiagent systems subject to disturbed leader's information," *IEEE Access*, vol. 8, pp. 227970–227981, 2020.

[33] H. Xiao and C. L. P. Chen, "Leader-follower consensus multi-robot formation control using neurodynamic-optimization-based nonlinear model predictive control," *IEEE Access*, vol. 7, pp. 43581–43590, 2019.

[34] Y. Jia and L. Wang, "Leader–follower flocking of multiple robotic fish," *IEEE/ASME Trans. Mechatronics*, vol. 20, no. 3, pp. 1372–1383, Jun. 2015.

[35] Q. Xie, Y. Xiao, X. Wang, D. Liu, and Z. Shen, "Heliostat cluster control for the solar tower power plant based on leader-follower strategy," *IEEE Access*, vol. 7, pp. 135031–135039, Jan. 2019.

[36] L. Zheng, S. X. Guo, Y. Piao, S. X. Gu, and R. An, "Collaboration and task planning of turtle-inspired multiple amphibious spherical robots," *Micromachines*, vol. 11, pp. 71–94, Jan. 2020.

PENG ZENG was born in Xiangyang, China, in 1988. He received the Bachelor of Science and Master of Science degrees from Guiyang University, Guiyang, China, in 2010 and 2013, respectively. His research interests include online environment monitoring system for power cable tunnels and robot control. He is currently a Researcher with the Electric Power Research Institute, Guizhou Power Grid Company Ltd., China.

JIAHONG HE was born in Nanjing, China, in 1988. He received the Bachelor of Science degree in electric engineering from Hohai University, Nanjing, in 2010, the Master of Science and Ph.D. degrees from Arizona State University, Tempe, USA. His research interests include the electric field computation using numerical methods in high voltage insulation and automation system for high voltage equipment. He is currently an Assistant Professor with Southeast University, China.

BINGTUAN GAO (Member, IEEE) received the B.E degree in electrical engineering and automation, the M.E. degree in control theory and control engineering, and the Ph.D. degree in power electronics and electrical drive from the Harbin Institute of Technology, Harbin, China, in 2002, 2004, and 2007, respectively. From 2008 to 2010, he held a postdoctoral position with the Department of Electrical and Computer Engineering, Michigan State University, East Lansing, USA. He is currently a Professor with the School of Electrical Engineering, Southeast University, Nanjing, China. His research interests include robotics, modelling and control of dynamic systems, renewable energy systems, and smart grids.

• • •